



**HAL**  
open science

# Photoelectrochemical Hydrogen Production by a Cobalt Tetrapyrrolyl Catalyst Using Push-Pull Dye-Sensitized NiO Photocathodes

Claire Bourguignon, Anthonin Moinel, Aurélien Huet, Yann Kervella,  
Christopher D. Windle, Julien Massin, Vincent Artero, Murielle  
Chavarot-Kerlidou, Renaud Demadrille

## ► To cite this version:

Claire Bourguignon, Anthonin Moinel, Aurélien Huet, Yann Kervella, Christopher D. Windle, et al.. Photoelectrochemical Hydrogen Production by a Cobalt Tetrapyrrolyl Catalyst Using Push-Pull Dye-Sensitized NiO Photocathodes. *Advanced Energy and Sustainability Research*, 2023, 4 (12), pp.2300095. 10.1002/aesr.202300095 . hal-04235646

**HAL Id: hal-04235646**

**<https://hal.science/hal-04235646v1>**

Submitted on 11 Oct 2023

**HAL** is a multi-disciplinary open access archive for the deposit and dissemination of scientific research documents, whether they are published or not. The documents may come from teaching and research institutions in France or abroad, or from public or private research centers.

L'archive ouverte pluridisciplinaire **HAL**, est destinée au dépôt et à la diffusion de documents scientifiques de niveau recherche, publiés ou non, émanant des établissements d'enseignement et de recherche français ou étrangers, des laboratoires publics ou privés.

# Photoelectrochemical Hydrogen Production by a Cobalt Tetrapyrrolyl Catalyst Using Push–Pull Dye-Sensitized NiO Photocathodes

Claire Bourguignon, Anthonin Moinel, Aurélien Huet, Yann Kervella, Christopher D. Windle, Julien Massin, Vincent Artero, Murielle Chavarot-Kerlidou,\* and Renaud Demadrille\*

Herein, the synthesis and optoelectronic properties of a novel push–pull organic dye, pRK1, specifically designed for use in dye-sensitized photocathodes for hydrogen generation, are reported. The chemical structure of this dye, which incorporates a benzothiadiazole moiety, is inspired by RK1, a dye previously reported as a photosensitizer in n-type dye-sensitized solar cells (DSSCs) with power conversion efficiencies above 10% and high stability. The photoelectrochemical activity for hydrogen evolution of pRK1 after grafting onto NiO photocathodes in combination with a cobalt tetrapyrrolyl catalyst  $[\text{Co}(\text{bapbpy})(\text{OH}_2)_2](\text{BF}_4)_2$  in aqueous solution is evaluated and compared with two reference dyes from the literature,  $\text{RuP}_2\text{-bpy}$  and P1. It is shown that among the three photocathodes studied in this work, NiO|pRK1 is the most efficient, producing up to  $1.9 \mu\text{mol cm}^{-2}$  of hydrogen with a faradaic efficiency of 66%, under visible light irradiation in aqueous electrolyte at pH 4.5. pRK1 shows a turnover number ( $\text{TON}_{\text{dye}}$ ) of up to 145 during the 6 h chronoamperometric test, almost twice that of P1. This study demonstrates that the chemical structure of high performance dyes commonly used in DSSCs can be successfully modified to meet the requirements for light-driven water splitting in dye-sensitized photoelectrochemical cells.

## 1. Introduction


The production of fuels and commodity chemicals from abundant molecules as feedstock ( $\text{H}_2\text{O}$ ,  $\text{CO}_2$ ,  $\text{O}_2$ ...) and sunlight as the primary energy source is a crucial challenge to meet the ever-growing energy demand in a more sustainable and carbon-neutral way. In this context, hydrogen ( $\text{H}_2$ ) production from water in photoelectrochemical cells (PECs) represents an emerging technological approach,<sup>[1]</sup> with solar-to-hydrogen (STH) conversion efficiencies above 10% recently achieved at the laboratory scale. However, these demonstrations rely on the combination of noble metal catalysts (Pt, Ir, Rh...) with solid-state light absorbers based on expensive and/or toxic metals (Ge, In, As...),<sup>[1–3]</sup> The anticipated shortage of these critical elements and the amount of raw materials needed to scale up these devices therefore raise serious concerns about the long-term sustainability of any large-scale development.<sup>[4]</sup>

Replacing expensive noble metals by earth-abundant elements while reducing the amount of raw materials is therefore highly demanded to develop cheap and sustainable water-splitting devices. Dye-sensitized photoelectrochemical cells (DS-PECs) are very promising in this regard;<sup>[5,6]</sup> they are based on the use of inexpensive, nontoxic semiconductor materials, a low-cost processing that can be easily scaled up, and the tunability of their molecular light-harvester and catalyst components, thus extending the concept of dye-sensitized solar cells (DSSCs).<sup>[7]</sup>

Organic dyes used to photosensitize metal oxides in DSSCs have been the subject of much research in recent years, and the development of molecules with tailored optoelectronic properties has led to significant improvements in the photoelectric performance of these devices. The vast majority of these organic dyes are based on a donor- $\pi$ -conjugated bridge-acceptor configuration. By exploiting the push–pull effect, where the donor moiety has a low ionization potential and the electron acceptor moiety has a high electron affinity, it is possible to control the positions of the highest occupied molecular orbital (HOMO) and lowest unoccupied molecular orbital (LUMO)

C. Bourguignon, A. Moinel, A. Huet, Y. Kervella, R. Demadrille  
Univ Grenoble Alpes, CNRS, CEA, IRIG, SYMMES  
17 rue des Martyrs, 38000 Grenoble, France  
E-mail: renaud.demadrille@cea.fr

C. Bourguignon, A. Moinel, C. D. Windle, J. Massin, V. Artero,  
M. Chavarot-Kerlidou  
Univ Grenoble Alpes, CNRS, CEA, IRIG, LCBM  
17 rue des Martyrs, 38000 Grenoble, France  
E-mail: murielle.chavarot-kerlidou@cea.fr

 The ORCID identification number(s) for the author(s) of this article can be found under <https://doi.org/10.1002/aesr.202300095>.

© 2023 The Authors. Advanced Energy and Sustainability Research published by Wiley-VCH GmbH. This is an open access article under the terms of the Creative Commons Attribution License, which permits use, distribution and reproduction in any medium, provided the original work is properly cited.

DOI: 10.1002/aesr.202300095

energy levels to meet the thermodynamic requirements of the system. Push–pull  $\pi$ -conjugated dyes have many advantages. They are generally easy to synthesize and have higher molar extinction coefficients than conventional noble complexes. These dyes can be a very attractive inspiration for improving the performance of DS-PECs. In addition, DS-PECs can also benefit from recent successes in bioinspired catalysis for energy-relevant applications to find alternatives to platinum group metal catalysts<sup>[8]</sup> and, today, several examples of H<sub>2</sub>-evolving photocathodes assembling molecular first row transition metal-based catalytic centers with push–pull organic dyes have been described in the literature.<sup>[9–24]</sup> However, up to now, the photoelectrochemical performances of these fully earth abundant systems remain relatively low. Strategies that would allow accelerating the screening and selection of promising dye and catalyst structures while providing structure–property relationships are thus highly needed to advance this field of research.

During the past decade, polypyridine cobalt complexes have emerged as an attractive family of H<sub>2</sub>-evolving catalysts, displaying high activities and stabilities in aqueous media.<sup>[25–27]</sup> We previously reported on homogeneous photocatalytic hydrogen production under fully aqueous conditions using a robust cobalt (II) polypyridyl complex [Co(bapbpy)(OH<sub>2</sub>)<sub>2</sub>](BF<sub>4</sub>)<sub>2</sub> (**1**(BF<sub>4</sub>)<sub>2</sub>, Figure 1).<sup>[28]</sup> In parallel, mechanistic studies highlighted the key role played by the tetradentate bis-aminopyridyl-bipyridine (bapbpy) ligand, bearing both a redox-active bipyridine moiety and pendant proton relays, in controlling the proton reduction mechanisms according to the operating conditions.<sup>[29]</sup> It therefore seems very relevant to evaluate the potential of this catalyst for photoelectrochemical hydrogen production in combination with push–pull dyes.

In this article, we report the synthesis and characterization of a novel organic dye coded **pRK1** (Figure 1), featuring a benzothiadiazole (BTD) unit. In designing this dye, we were strongly inspired by **RK1**, a push–pull dye used in n-DSSCs that has demonstrated conversion efficiencies of more than 10% with a

stability of more than 9000 h in accelerated device tests.<sup>[30]</sup> Our aim was to test whether the simple structure of **RK1** could be adapted for the sensitization of NiO photocathodes, resulting in **pRK1**. The hydrogen-evolving photoelectrochemical activity of **pRK1**-sensitized NiO photocathodes was assessed in combination with **1**(BF<sub>4</sub>)<sub>2</sub> in solution, and these performances were benchmarked against two reference dye structures from the field, **RuP<sub>2</sub>-bpy** and **P1**.

## 2. Results and Discussion

### 2.1. Design and Synthesis of the New Dye **pRK1**

In order to obtain a new dye with suitable optoelectronic properties for the fabrication of efficient photocathodes on NiO films, we designed a push–pull molecular architecture based on a BTD unit. For the design, we were inspired by the chemical structure of **RK1**, a dye that has shown remarkable photoelectrical performance and stability in DSSCs.<sup>[30,31]</sup> In recent years, **RK1**-inspired dyes have been reported for use in a heterogeneous photocatalytic hydrogen production system.<sup>[21,32]</sup> Hence, for the construction of the new dye, we used a triphenylamine (TPA) unit functionalized with two carboxylic acids as the electron donor group. Like phosphonic acid,<sup>[33]</sup> carboxylic acid functions have been shown to lead to robust anchoring on NiO electrodes.<sup>[34,35]</sup> This unit was linked to the BTD electron donor group via an *n*-octyl-thiophene as a  $\pi$ -conjugated spacer and on the other side we introduced a cyano-acrylamide function.

The synthetic route toward the dye **pRK1** is described in Scheme 1. The synthesis is relatively simple and is performed in six steps. This dye is obtained with an overall yield of 28% starting from building blocks described in previous work, i.e., 4-(7-bromobenzo[*c*][1,2,5]thiadiazol-4-yl)benzaldehyde (**5**), the 2-cyano-*N*-(prop-2-yn-1-yl)acetamide (**7**), di-*tert*-butyl 4,4'-((4-(4,4,5,5-tetramethyl-1,3,2-dioxaborolan-2-yl)phenyl)azanediyl)dibenzoate (**1**). The synthesis starts with a Suzuki–Miyaura

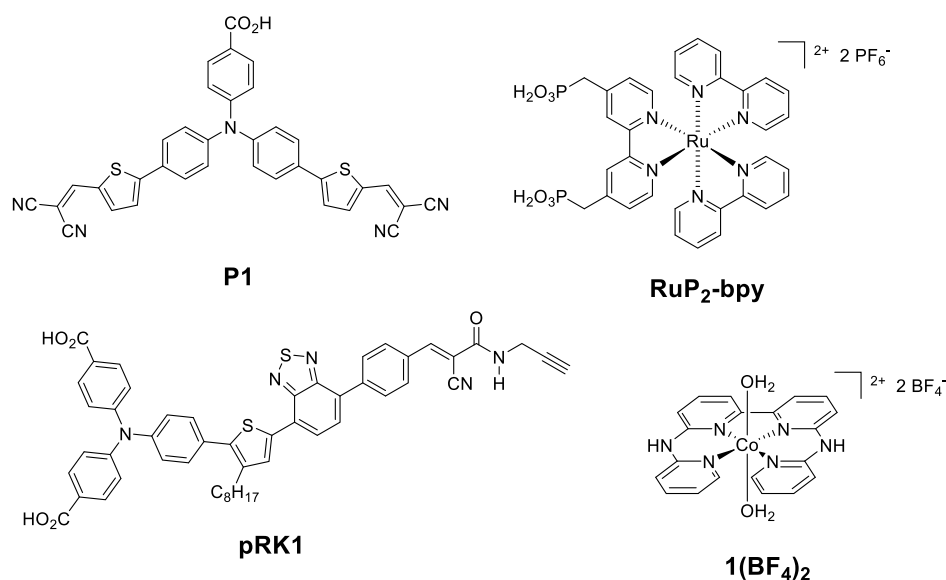
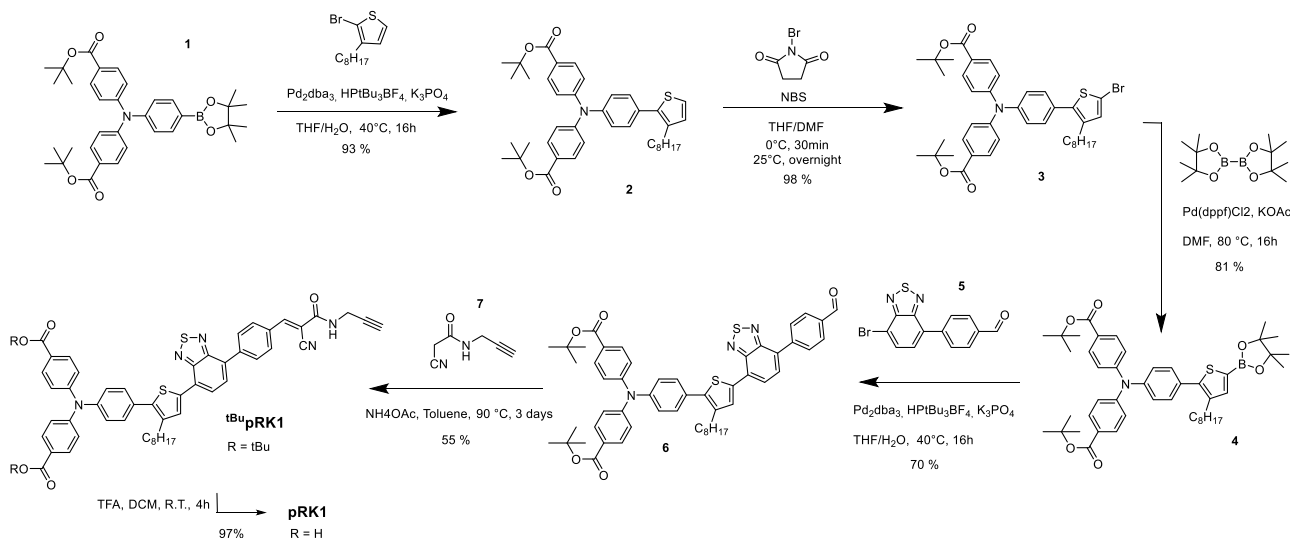


**Figure 1.** Structures of the dyes **P1**, **RuP<sub>2</sub>-bpy**, and **pRK1** and of the catalyst [Co(bapbpy)(OH<sub>2</sub>)<sub>2</sub>](BF<sub>4</sub>)<sub>2</sub> (**1**(BF<sub>4</sub>)<sub>2</sub>) employed in this study.

coupling between the TPA-derivative **1** and 2-bromo-3-octylthiophene to give compound **2** in 93% yield after purification on a silica gel by chromatography. The free  $\alpha$  position of the thiophene is then almost quantitatively brominated with NBS under mild conditions to give compound **3**. The borylation of the latter is carried out in a pallado-catalyzed reaction with  $B_2pin_2$ , to give the corresponding borylated compound **4**. This molecule is coupled to compound **5** by a Suzuki–Miyaura coupling reaction to give the aldehyde **6**. In our experience, the chosen Suzuki coupling conditions used to obtain compound **2** are versatile and allowed us to obtain compound **6** in 70% yield. At this stage the push–pull structure is obtained, resulting in a color change of the compounds from pale yellow to dark orange. Finally, a Knoevenagel condensation is performed under mild conditions between aldehyde **6** and compound **7**. The *tert*-butyl-protected compound  $tBu_pRK1$  is thus obtained after purification on a silica gel by chromatography under the form of a red–orange solid, used for all the characterizations in solution. The last step, corresponding to the deprotection of the anchoring functions to yield  $pRK1$ , is performed just before the grafting of the molecule. The final dye is recovered quantitatively by action of trifluoroacetic acid (TFA) as shown by NMR spectroscopy and used without further purification. All the synthesis procedures and characterizations of the intermediates are reported in Supporting Information.

## 2.2. Optoelectronic Properties of $tBu_pRK1$ in Solution and Thermodynamic Consideration

The UV–vis absorption spectrum of  $tBu_pRK1$  was recorded in DCM at 25 °C and compared to the ones of **P1** and  $RuP_2^{OEt-bpy}$  (Figure 2). The optical and electronic properties of all compounds are gathered and compared in Table 1. We have characterized the dye in its ester form  $tBu_pRK1$  in order to better mimic the properties of the dye covalently anchored onto the NiO surface, i.e., through reaction of the carboxylic acids in  $pRK1$  with Ni-OH surface hydroxyl groups to form nickel-carboxylate bonds.



Scheme 1. Synthetic route and conditions for the preparation of  $pRK1$ .

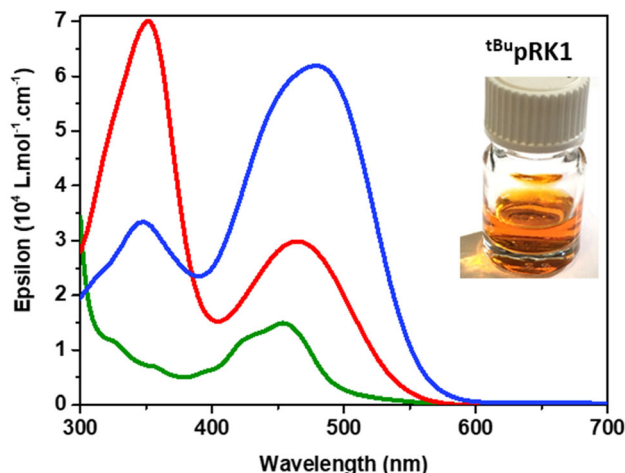


Figure 2. UV–vis absorption spectra of  $tBu_pRK1$  (red line, recorded in DCM) and **P1** (blue line, recorded in DCM), and  $RuP_2^{OEt-bpy}$  (green line, recorded in MeCN) and picture of a  $tBu_pRK1$  solution.

Of the three dyes, the ruthenium-based  $RuP_2-bpy$  shows the poorest absorption properties. This result is expected because in this class of compounds the absorption band in the visible is mainly based on an metal to ligand charge transfer (MLCT) transition<sup>[36,37]</sup> which is known to give rise to low molar absorption coefficient. On the contrary, the new purely organic dye  $tBu_pRK1$  based on a push–pull chemical design shows an improved absorption with quite similar properties when compared to **P1**. Indeed, **P1** and  $tBu_pRK1$  exhibit two absorption peaks, one located at around 350 nm in the UV region and a second one that is found at 478 nm for **P1** and 465 nm for  $tBu_pRK1$ . The absorption band in the UV region is originating from  $\pi-\pi^*$  transition whereas the broad absorption band located in the visible range originates from an intramolecular charge transfer (ICT) transition. In  $tBu_pRK1$ , the molar extinction coefficient of the UV-band is more than doubled compared to the one of **P1**.

**Table 1.** Photophysical and redox properties of  $\text{RuP}_2^{\text{OEt-bpy}}$ , **P1**, and  ${}^{\text{tBu}}\text{pRK1}$ .

	$\lambda_1$ [e] <sup>a)</sup>	$\lambda_2$ [e] <sup>a)</sup>	$E_{00}$ [eV] <sup>b)</sup>	Dye <sup>+</sup> /Dye <sup>c)</sup>	Dye/Dye <sup>-c)</sup>
$\text{RuP}_2^{\text{OEt-bpy}}$ <sup>[44]</sup>	–	453 (14 918)	2.12	+1.40	–1.20
<b>P1</b> <sup>[48]</sup>	347 <sup>d)</sup> (33 247)	478 <sup>d)</sup> (61 935)	2.25	+1.38	–0.77
${}^{\text{tBu}}\text{pRK1}$	351 (70 003)	465 (29 857)	2.21	+1.12	–1.14

<sup>a)</sup> $\lambda$  in nm,  $\epsilon$  in  $\text{M}^{-1} \text{cm}^{-1}$ ; <sup>b)</sup>0–0 transition energy estimated from the intercept of the normalized absorption and emission spectra (see Figure S2, Supporting Information); <sup>c)</sup>In V versus NHE (redox potentials converted from  $\text{Fc}^{+/0}$  to NHE considering  $E^\circ(\text{Fc}^{+/0}) = +0.53 \text{ V}$  versus NHE in acetonitrile and  $+0.54 \text{ V}$  versus NHE in dichloromethane);<sup>[49]</sup> this value is corrected for the interliquid potential  $E_{\text{L,S}}$  between the aqueous NHE and the organic supporting electrolyte;<sup>[50]</sup> <sup>d)</sup>This work, **P1** values measured in DCM.

This is due to the presence of additional aromatic and heteroaromatic units in the structure such as the thiophene and BTd, leading to a more extended  $\pi$ -conjugated system. On the other hand,  ${}^{\text{tBu}}\text{pRK1}$  shows an ICT absorption band that is hypsochromically shifted in the visible (by 13 nm) compared to **P1** and the molar extinction coefficient of its ICT absorption band is almost reduced by a factor two compared to the one of **P1**. The presence of two malononitrile functions as electron withdrawing groups, containing each two cyano units, can explain the higher intensity of the ICT band.<sup>[38,39]</sup>

To get more insights into the optoelectronic properties of the new dye  ${}^{\text{tBu}}\text{pRK1}$ , cyclic voltammetry (CV) experiments were carried out with the goal to determine the potentials for its first reduction and oxidation (Figure S3, Supporting Information). From these potentials we estimated the HOMO and LUMO energy levels that were compared to the ones obtained from the modeling by density functional theory (DFT) calculation using the ADF 2016 package.<sup>[40]</sup> These measurements and calculations are necessary to verify that the electronic and redox properties of the new dye comply with the thermodynamic requirements for photoelectrochemical hydrogen production.

${}^{\text{tBu}}\text{pRK1}$  exhibits two reversible oxidation waves located at  $+0.58$  and  $+0.85 \text{ V}$  versus  $\text{Fc}^{+/0}$  ( $+1.12$  and  $+1.39 \text{ V}$  vs NHE), positioning the HOMO level around  $-5.62 \text{ eV}$ , in good agreement with the value of  $-5.36 \text{ eV}$  obtained from the modeling. Looking at the spatial localization of the electronic density (Figure 3), it clearly appears that the TPA unit dictates the HOMO energy-level position. When scanning toward negative potentials,  ${}^{\text{tBu}}\text{pRK1}$  exhibits an irreversible reduction peak with a reduction edge at around  $-1.68 \text{ V}$  versus  $\text{Fc}^{+/0}$  ( $-1.14 \text{ V}$  vs NHE). DFT modeling shows that the spatial localization of the LUMO extends from the thiophene unit to the nitrogen of the 2-cyano-*N*-(prop-2-yn-1-yl)acetamide. The LUMO energy level is found experimentally at around  $-3.36$  and at  $-2.99 \text{ eV}$  from DFT.

On this basis, the driving force  $\Delta G_{\text{inj}}$  for hole injection from the new dye  ${}^{\text{tBu}}\text{pRK1}$  excited state to the NiO valence band is estimated to be  $-0.60 \text{ eV}$  (with  $E_{\text{FB}}$  (NiO) =  $+0.52 \text{ V}$  vs NHE at pH 4.5),<sup>[41]</sup> and the reduction of the Co(II) complex  $1(\text{BF}_4)_2$  is thermodynamically allowed with a minimum driving force of  $-0.34 \text{ eV}$ . Note that the NiO valence band edge potential at this pH was estimated from the value of  $0.37 \text{ V}$  versus NHE

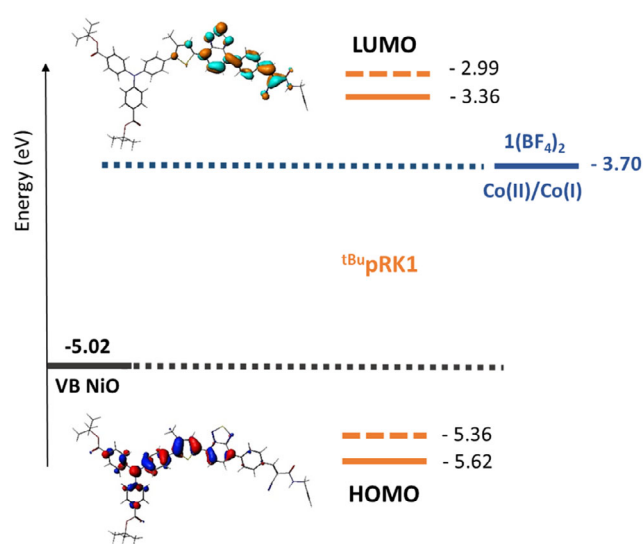


**Figure 3.** Energetic and spatial positioning of the HOMO and LUMO boundary orbitals of  ${}^{\text{tBu}}\text{pRK1}$  measured (solid line) and modeled by DFT calculation (dashed line). Energetic position of the NiO valence band, as well as of the Co(II)/Co(I) redox couple for  $1(\text{BF}_4)_2$ ,<sup>[28]</sup> potentials converted according to  $E \text{ (eV)} = -4.50 - E \text{ (V vs NHE)}$ .<sup>[46,47]</sup>

determined by Natu and co-workers<sup>[40]</sup> at pH 7 and is in agreement with other experimental values from the literature.<sup>[42]</sup>

### 2.3. Photoelectrochemical Performances for Hydrogen Production

In order to evaluate the photoelectrochemical activity of the new dye in combination with the cobalt catalyst  $1(\text{BF}_4)_2$ , we prepared dye-sensitized mesoporous NiO electrodes. NiO is a wide bandgap p-type semiconductor material with a bandgap energy between 3.6 and 4.0 eV depending on the preparation method and although this material has a low intrinsic hole mobility, it is so far the dominant p-type semiconductor for the preparation of dye-sensitized photocathodes.<sup>[43]</sup> F108-templated mesoporous NiO films were prepared by a sol-gel process and deposited onto conductive FTO glass by spin coating according to our previously reported procedures, describing the procedure and the characterization of these films.<sup>[11,16]</sup> The films were sensitized by soaking for 24 h in a solution of dye (either  $\text{RuP}_2\text{-bpy}$ , **P1**, or **pRK1**) and the dye loading was determined for each individual sample (full details in the Supporting Information).

The photoelectrochemical activity of the dye-sensitized NiO films was investigated in a three-electrode configuration setup, in the presence of  $1(\text{BF}_4)_2$  (1 mM) in solution in an aqueous sodium acetate buffer electrolyte at pH 4.5; these experimental conditions were chosen according to a related study using the cobaloxime catalyst  $[\text{Co}(\text{dmgBF}_2)_2(\text{OH})_2]$  in solution. Moreover, the light-driven  $\text{H}_2$  production activity of  $1(\text{BF}_4)_2$  was previously reported under homogeneous aqueous conditions at a very close pH (pH 4).<sup>[28]</sup> Linear sweep voltammograms were first recorded from  $+1$  to  $0 \text{ V}$  versus RHE in the dark and under visible light irradiation conditions. All systems generate cathodic photocurrents with high positive onset potentials ( $+0.9 \text{ V}$  vs RHE



for NiO|**pRK1**, +0.7 V vs RHE for NiO|**RuP<sub>2</sub>-bpy** and NiO|**P1**, albeit with significant differences in their magnitude (Figure S4, Supporting Information). In order to more accurately compare the performances of the different dye-sensitized photocathodes, steady-state photocurrents were recorded at an applied potential of +0.07 V versus RHE (−0.4 V vs Ag/AgCl) under chopped-light irradiation (Figure 4 and S5, Supporting Information). A control experiment on a blank NiO film confirmed the absence of current when the light is switched on (Figure 4 top, gray line), confirming that NiO sensitization by a visible-light absorbing dye is a prerequisite for photocurrent generation. Significant differences are, however, observed when comparing the photoelectrochemical activities of the three different dye-sensitized films: photocurrent densities of −15 and −20  $\mu\text{A cm}^{-2}$  are generated by NiO|**P1** and NiO|**pRK1**, respectively, whereas only −2  $\mu\text{A cm}^{-2}$  is recorded on NiO|**RuP<sub>2</sub>-bpy**. For the latter, a similar value is measured in the absence of the cobalt complex in solution, while the presence of **1(BF<sub>4</sub>)<sub>2</sub>** in solution results in a fourfold to fivefold increase in the photocurrent densities for NiO|**P1** and NiO|**pRK1** (Figure S5, Supporting Information); moreover, the photogenerated charges are efficiently extracted by the cobalt catalyst, as evidenced by the absence of any anodic spike on the photocurrent traces when the light is switched off (Figure 4a).<sup>[22]</sup>

The photocurrent densities normalized to the dye loading provide a more meaningful analysis of the data (Figure 4b), allowing comparison of the intrinsic activities of each dye. Thus, although the thermodynamic driving forces for hole injection and cobalt reduction are very similar for **pRK1** and **RuP<sub>2</sub>-bpy**, the latter display a threefold lower activity (−0.9  $\mu\text{A nmol}_{\text{dye}}^{-1}$  for NiO|**RuP<sub>2</sub>-bpy** vs −2.8  $\mu\text{A nmol}_{\text{dye}}^{-1}$  for NiO|**pRK1**). Two parameters can account for this observation: first, the light absorption efficiency in the visible region is higher for **pRK1**, compared to **RuP<sub>2</sub>-bpy** (Figure 2); second, the push–pull architecture in **pRK1** allows spatial charge separation, i.e., the photogenerated electron is moved away from the NiO surface, which, in turn, favors the forward electron transfer to the catalyst present in the electrolyte solution. Such a spatial charge delocalization cannot occur with the **RuP<sub>2</sub>-bpy** structure,<sup>[44]</sup> and in that case the lack of photoelectrochemical activity when **1(BF<sub>4</sub>)<sub>2</sub>** is present in solution can be rationalized by a charge recombination process

between the reduced dye and the NiO electrode faster than the forward electron transfer.

On the other hand, the intrinsic activity of **pRK1** is more than twice as high as that of **P1** (−2.8 vs −1.2  $\mu\text{A nmol}_{\text{dye}}^{-1}$ , respectively). This value directly reflects the overall electron transfer kinetics mediated by the dye at the electrode–electrolyte interface, which is therefore more than twice faster for NiO|**pRK1** compared to NiO|**P1**. This observation goes against the light absorption efficiency in the visible region, which is much higher for **P1** than for **pRK1** (Figure 2), and thus underlines that additional parameters need to be taken into account to rationalize the differences in photoelectrochemical activity between the two systems. Obviously, the nature of the pi-conjugated spacer is different in **pRK1** and **P1**; the presence of the BTD unit might increase the lifetime of the charge-separated state, making electron transfer to the cobalt center more efficient. In addition, the organization of the dye molecules at the surface of the NiO film most likely affects the performances; one known deactivation pathway for push–pull dyes is induced by aggregation upon immobilization on the semiconductor surface, which opens the way for inter-dye quenching of the excited state. Such aggregation is likely reduced for NiO|**pRK1**, compared to NiO|**P1**, thanks to the introduction of the lateral octyl chain on the thiophene unit in **pRK1**.

To confirm the origin of the observed photocurrents, chronoamperometric measurements were performed at +0.07 V versus RHE (−0.4 V vs Ag/AgCl) under continuous visible light irradiation for 6 h (Figure S6–S8, Supporting Information). The amount of hydrogen produced was quantified at the end of the experiment both in the headspace and in solution, according to our previously reported studies.<sup>[22]</sup> This allows determining a faradaic efficiency (FE) for hydrogen production and to calculate the turnover numbers ( $\text{TON}_{\text{dye}}$ ) achieved by the different dye-sensitized photocathodes. The data are summarized in Table 2 (full set of data in Table S1, Supporting Information).

As expected from the steady-state photocurrent measurements discussed above, NiO|**pRK1** is the most effective photocathode, producing 1.9  $\mu\text{mol cm}^{-2}$  of hydrogen with a Faradaic efficiency of 66%; 145  $\text{TON}_{\text{dye}}$  are achieved by **pRK1** during the course of the 6 h experiments, which is almost double compared to **P1**.

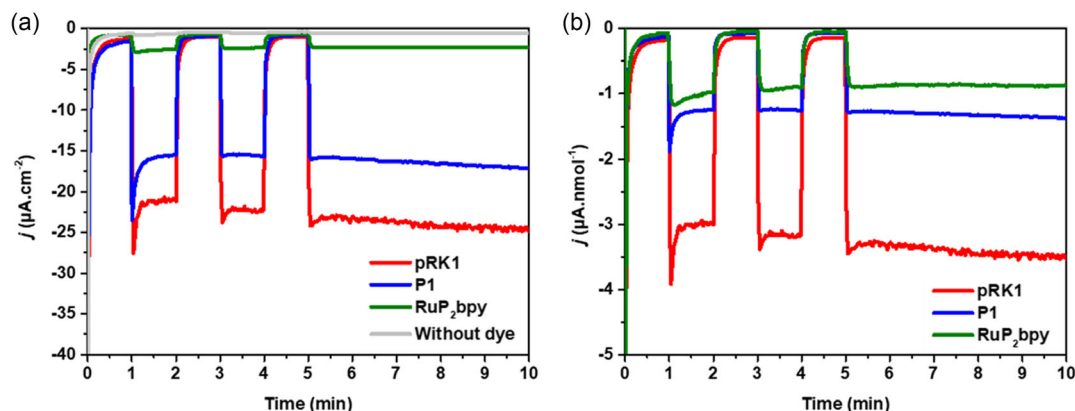


**Figure 4.** a) Chopped-light chronoamperometric measurements recorded on NiO (gray line), NiO|**RuP<sub>2</sub>-bpy** (green line), NiO|**P1** (blue line), and NiO|**pRK1** (red line) photocathodes at +0.07 V versus RHE (−0.4 V vs Ag/AgCl) in the presence of **1(BF<sub>4</sub>)<sub>2</sub>** (1 mM) in acetate buffer (0.1 M) pH 4.5. b) Photocurrent densities normalized to the dye loading.

**Table 2.** Figures of merit determined from 6 h chronoamperometric measurements in acetate buffer (0.1 M, pH 4.5) at an applied potential of +0.07 V versus RHE (−0.4 V vs Ag/AgCl). Maximum values and average values over two experiments in parenthesis.

	Dye loading [nmol cm <sup>−2</sup> ]	<b>1</b> [BF <sub>4</sub> ] <sub>2</sub> [mM]	Q [mC cm <sup>−2</sup> ]	nH <sub>2</sub> [nmol cm <sup>−2</sup> ]	F.E. [%]	TON <sub>dye</sub>
NiO	–	1	15	2	<5	–
NiO  <b>RuP</b> <sub>2</sub> - <b>bpy</b>	2.8 ± 0.1	0	52	3	<5	≈1
		1	96 (94)	3 (3)	<5	≈1
NiO  <b>P1</b>	11.9 ± 1.3	0	92	46	10	4
		1	314 (302)	923 (846)	57 (54)	74 (74)
NiO  <b>pRK1</b>	9.0 ± 3.6	0	52	8	<5	≈1
		1	549 (432)	1884 (1383)	66 (59)	145(135)

Notably, these performances are much better than those previously recorded with a related dye-sensitized photocathode in the presence of the cobaloxime catalyst [Co(dmgbF<sub>2</sub>)<sub>2</sub>(OH)<sub>2</sub>] in solution.<sup>[45]</sup>

Control experiments recorded either on a blank NiO film or in the absence of **1**(BF<sub>4</sub>)<sub>2</sub> in the electrolyte produced only traces of H<sub>2</sub> compared to NiO|**P1** and NiO|**pRK1**. These observations clearly support a cobalt-based mechanism for the observed hydrogen production activity. In contrast, the amount of hydrogen produced by NiO|**RuP**<sub>2</sub>-**bpy** over the course of the 6 h experiment lies in the same range than the two control experiments, confirming that **RuP**<sub>2</sub>-**bpy** is not able to activate the catalyst in solution, as charge recombination between the reduced dye and the hole in NiO is most likely faster than forward electron transfer to the cobalt center.

### 3. Conclusion

In conclusion, we have designed, synthesized, and characterized a novel metal-free organic dye based on a benzothiadiazole moiety, **pRK1**, for the preparation of dye-sensitized photocathodes. The new dye was obtained in six steps and shows a good absorption in the visible region with an absorption edge close to 575 nm in dichloromethane solution. In addition, its HOMO and LUMO energy levels are well positioned, on the one hand, to efficiently sensitize NiO employed as photocathode material and, on the other hand, to effectively transfer electrons to the cobalt(II) polypyridyl complex **1**(BF<sub>4</sub>)<sub>2</sub>. The photoelectrochemical activity for hydrogen evolution of **pRK1**-sensitized NiO photocathodes was therefore evaluated and the performance of **pRK1** was benchmarked with two reference dyes, **RuP**<sub>2</sub>-**bpy**, a ruthenium-based dye and **P1**, another purely organic dye. We found that NiO|**pRK1** is the most efficient photocathode, producing up to 1.9 μmol cm<sup>−2</sup> of hydrogen with a faradaic efficiency of 66%, under visible light irradiation in aqueous electrolyte at pH 4.5; 135 ± 14 TON<sub>dye</sub> are achieved by **pRK1** during the course of 6 h chronoamperometric experiments, which is almost double compared to **P1**, in excellent agreement with the higher photocurrents (normalized to the dye loading) recorded on NiO|**pRK1**. This demonstrates that the chemical structure of high-performance dyes commonly used in DSSCs can be successfully modified to meet the requirements for light-driven

water splitting in DS-PECs. This work also highlights that working with robust hydrogen-evolving catalysts such as **1**(BF<sub>4</sub>)<sub>2</sub> is essential to evaluate and compare the performance of a range of dye-sensitized photocathodes in a meaningful way.

### Supporting Information

Supporting Information is available from the Wiley Online Library or from the author.

### Acknowledgements

C.B. and A.M. contributed equally to this work. This work was supported by the French National Research Agency (Labex ARCANE, CBH-EUR-GS, ANR-17-EURE-0003) and the CEA through the DRF-Impulsion program. A.M. acknowledges CEA for funding through a CFR Ph.D. grant. R.D. acknowledges the European Research Council (ERC) for funding. This work was partially funded under the European Union's Horizon 2020 Research and Innovation Program (grant agreement no. 832606; project PISCO). The authors thank Dr. P. Maldivi for her help with the DFT calculations. The authors thank Dr. C. Aumaitre for helpful discussions.

### Conflict of Interest

The authors declare no conflict of interest.

### Author Contributions

A.M. and A.H. synthesized and characterized the dye; Y.K. synthesized precursors **5** and **7**. C.B. carried out the photoelectrochemical measurements; A.M. performed the quantum chemical calculations (investigation–methodology–visualization). J.M. and C.W. performed the photoelectrochemical measurements of the ruthenium dye (investigation–methodology). R.D., V.A., and M.C.K. supervised the work, designed the materials and experiments, analyzed the data (supervision–validation). R.D. and M.C.K. obtained the funding for this work (conceptualization–funding acquisition–analysis–methodology–supervision–validation–writing–editing). All authors contributed to the work and gave approval to the final version of the manuscript.

### Data Availability Statement

The data that support the findings of this study are available in the supplementary material of this article.

### Keywords

cobalt catalysts, dye-sensitized photocathodes, hydrogen production, organic dyes

Received: June 1, 2023  
Revised: August 31, 2023  
Published online:

- [1] J. H. Kim, D. Hansora, P. Sharma, J.-W. Jang, J. S. Lee, *Chem. Soc. Rev.* **2019**, *48*, 1908.
- [2] W.-H. Cheng, M. H. Richter, M. M. May, J. Ohlmann, D. Lackner, F. Dimroth, T. Hannappel, H. A. Atwater, H.-J. Lewerenz, *ACS Energy Lett.* **2018**, *3*, 1795.

- [3] S. Tembhurne, F. Nandjou, S. Haussener, *Nat. Energy* **2019**, 4, 399.
- [4] P. C. K. Vesborg, T. F. Jaramillo, *RSC Adv.* **2012**, 2, 7933.
- [5] S. Zhang, H. Ye, J. Hua, H. Tian, *EnergyChem* **2019**, 1, 100015.
- [6] Z. Yu, F. Li, L. Sun, *Energy Environ. Sci.* **2015**, 8, 760.
- [7] A. B. Muñoz-García, I. Benesperi, G. Boschloo, J. J. Concepcion, J. H. Delcamp, E. A. Gibson, G. J. Meyer, M. Pavone, H. Pettersson, A. Hagfeldt, M. Freitag, *Chem. Soc. Rev.* **2021**, 50, 12450.
- [8] R. M. Bullock, J. G. Chen, L. Gagliardi, P. J. Chirik, O. K. Farha, C. H. Hendon, C. W. Jones, J. A. Keith, J. Klosin, S. D. Minter, R. H. Morris, A. T. Radosevich, T. B. Rauchfuss, N. A. Strotman, A. Vojvodic, T. R. Ward, J. Y. Yang, Y. Surendranath, *Science* **2020**, 369, 786.
- [9] L. Li, L. Duan, F. Wen, C. Li, M. Wang, A. Hagfeldt, L. Sun, *Chem. Commun.* **2012**, 48, 988.
- [10] F. Li, K. Fan, B. Xu, E. Gabrielsson, Q. Daniel, L. Li, L. Sun, *J. Am. Chem. Soc.* **2015**, 137, 9153.
- [11] N. Kaeffer, J. Massin, C. Lebrun, O. Renault, M. Chavarot-Kerlidou, V. Artero, *J. Am. Chem. Soc.* **2016**, 138, 12308.
- [12] N. Kaeffer, C. D. Windle, R. Brisse, C. Gablin, D. Leonard, B. Jusselme, M. Chavarot-Kerlidou, V. Artero, *Chem. Sci.* **2018**, 9, 6721.
- [13] P. B. Pati, L. Zhang, B. Philippe, R. Fernández-Terán, S. Ahmadi, L. Tian, H. Rensmo, L. Hammarström, H. Tian, *ChemSusChem* **2017**, 10, 2480.
- [14] C. D. Windle, H. Kumagai, M. Higashi, R. Brisse, S. Bold, B. Jusselme, M. Chavarot-Kerlidou, K. Maeda, R. Abe, O. Ishitani, V. Artero, *J. Am. Chem. Soc.* **2019**, 141, 9593.
- [15] N. Lalaoui, M. Abdellah, K. L. Materna, B. Xu, H. Tian, A. Thapper, J. Sa, L. Hammarström, S. Ott, *Dalton Trans.* **2022**, 51, 15716.
- [16] A. Moinel, M. Brochnow, C. Aumaitre, E. Giannoudis, J. Fize, C. Saint-Pierre, J. Pécaut, P. Maldivi, V. Artero, R. Demadrille, M. Chavarot-Kerlidou, *Sustainable Energy Fuels* **2022**, 6, 3565.
- [17] C. E. Creissen, J. Warnan, E. Reisner, *Chem. Sci.* **2018**, 9, 1439.
- [18] C. E. Creissen, J. Warnan, D. Antón-García, Y. Farré, F. Odobel, E. Reisner, *ACS Catal.* **2019**, 9, 9530.
- [19] K. L. Materna, A. M. Beiler, A. Thapper, S. Ott, H. Tian, L. Hammarström, *ACS Appl. Mater. Interfaces* **2020**, 12, 31372.
- [20] K. A. Click, D. R. Beauchamp, Z. Huang, W. Chen, Y. Wu, *J. Am. Chem. Soc.* **2016**, 138, 1174.
- [21] L. Nhon, B. Shan, A. D. Taggart, R. M. W. Wolfe, T.-T. Li, C. M. Klug, A. Nayak, R. M. Bullock, J. F. Cahoon, T. J. Meyer, K. S. Schanze, J. R. Reynolds, *ACS Appl. Mater. Interfaces* **2021**, 13, 47499.
- [22] S. Bold, J. Massin, E. Giannoudis, M. Koepf, V. Artero, B. Dietzek, M. Chavarot-Kerlidou, *ACS Catal.* **2021**, 11, 3662.
- [23] Y. Bentounsi, K. Seintis, S. Diring, E. Vauthey, F. Odobel, *ACS Appl. Energy Mater.* **2021**, 4, 2629.
- [24] Y. Yu, K. A. Click, S. M. Polen, M. He, C. M. Hadad, Y. Wu, *J. Phys. Chem. C* **2017**, 121, 20720.
- [25] F. Droghetti, F. Lucarini, A. Molinari, A. Ruggi, M. Natali, *Dalton Trans.* **2022**, 51, 10658.
- [26] L. Tong, L. Duan, A. Zhou, R. P. Thummel, *Coord. Chem. Rev.* **2020**, 402, 213079.
- [27] D. Z. Zee, T. Chantarojsiri, J. R. Long, C. J. Chang, *Acc. Chem. Res.* **2015**, 48, 2027.
- [28] N. Queyriaux, E. Giannoudis, C. D. Windle, S. Roy, J. Pécaut, A. G. Coutsolelos, V. Artero, M. Chavarot-Kerlidou, *Sustainable Energy Fuels* **2018**, 2, 553.
- [29] N. Queyriaux, D. Sun, J. Fize, J. Pécaut, M. J. Field, M. Chavarot-Kerlidou, V. Artero, *J. Am. Chem. Soc.* **2020**, 142, 274.
- [30] D. Joly, L. Pellejà, S. Narbey, F. Oswald, J. Chiron, J. N. Clifford, E. Palomares, R. Demadrille, *Sci. Rep.* **2014**, 4, 4033.
- [31] D. Joly, L. Pellejà, S. Narbey, F. Oswald, T. Meyer, Y. Kervella, P. Maldivi, J. N. Clifford, E. Palomares, R. Demadrille, *Energy Environ. Sci.* **2015**, 8, 2010.
- [32] M. Bartolini, V. Gombac, A. Sinicropi, G. Reginato, A. Dessì, A. Mordini, J. Filippi, T. Montini, M. Calamante, P. Fornasiero, L. Zani, *ACS Appl. Energy Mater.* **2020**, 3, 8912.
- [33] K. L. Materna, R. H. Crabtree, G. W. Brudvig, *Chem. Soc. Rev.* **2017**, 46, 6099.
- [34] Y. Farré, F. Maschietto, J. Föhlinger, M. Wykes, A. Planchat, Y. Pellegrin, E. Blart, I. Ciofini, L. Hammarström, F. Odobel, *ChemSusChem* **2020**, 13, 1844.
- [35] K. W. Wulser, M. A. Langell, *Catal. Lett.* **1992**, 15, 39.
- [36] M. K. Nazeeruddin, C. Klein, P. Liska, M. Grätzel, *Coord. Chem. Rev.* **2005**, 249, 1460.
- [37] T. Shimamura, A. Kobayashi, Y. Oaki, M. Yoshida, M. Kato, *Energy Fuels* **2022**, 36, 11559.
- [38] F. Baert, C. Cabanetos, M. Allain, V. Silvestre, P. Leriche, P. Blanchard, *Org. Lett.* **2016**, 18, 1582.
- [39] K. Erden, C. Dengiz, *J. Org. Chem.* **2022**, 87, 4385.
- [40] ADF SCM, *Theoretical Chemistry*, Vrije Universiteit, Amsterdam, The Netherlands, <https://www.scm.com>.
- [41] G. Natu, P. Hasin, Z. Huang, Z. Ji, M. He, Y. Wu, *ACS Appl. Mater. Interfaces* **2012**, 4, 5922.
- [42] M. A. Gross, C. E. Creissen, K. L. Orchard, E. Reisner, *Chem. Sci.* **2016**, 7, 5537.
- [43] C. J. Wood, G. H. Summers, C. A. Clark, N. Kaeffer, M. Braeutigam, L. R. Carbone, L. D'Amario, K. Fan, Y. Farré, S. Narbey, F. Oswald, L. A. Stevens, C. D. J. Parmenter, M. W. Fay, A. L. Torre, C. E. Snape, B. Dietzek, D. Dini, L. Hammarström, Y. Pellegrin, F. Odobel, L. Sun, V. Artero, E. A. Gibson, *Phys. Chem. Chem. Phys.* **2016**, 18, 10727.
- [44] N. Queyriaux, R. A. Wahyuono, J. Fize, C. Gablin, M. Wächtler, E. Martinez, D. Léonard, B. Dietzek, V. Artero, M. Chavarot-Kerlidou, *J. Phys. Chem. C* **2017**, 121, 5891.
- [45] J. Massin, M. Bräutigam, S. Bold, M. Wächtler, M. Pavone, A. B. Muñoz-García, B. Dietzek, V. Artero, M. Chavarot-Kerlidou, *J. Phys. Chem. C* **2019**, 123, 17176.
- [46] *Handbook of Electrochemistry* (Ed: C. G. Zoski), Elsevier, Amsterdam **2007**.
- [47] A. J. Bard, L. R. Faulkner, *Electrochemical Methods: Fundamentals and Applications*, 2nd ed., Wiley **2000**.
- [48] P. Qin, H. Zhu, T. Edvinsson, G. Boschloo, A. Hagfeldt, L. Sun, *J. Am. Chem. Soc.* **2008**, 130, 8570.
- [49] T. N. Huan, R. T. Jane, A. Benayad, L. Guetaz, P. D. Tran, V. Artero, *Energy Environ. Sci.* **2016**, 9, 940.
- [50] C. Costentin, S. Drouet, M. Robert, J.-M. Savéant, *Science* **2012**, 338, 90.